Measurement-Based Performance Evaluation of MIMO HSDPA

Christian Mehlführer, *Member, IEEE*, Sebastian Caban, *Member, IEEE*, and Markus Rupp, *Senior Member, IEEE*

***Abstract*—In this paper, we report on the results of physical-layer multiple-input–multiple-output High-Speed Downlink Packet Access (HSDPA) throughput measurements. These measurements were carried out in two different environments: 1) an alpine valley and 2) a city. In addition to the standard compliant single- and two-transmit-antenna HSDPA schemes, we defined and measured a four-transmit-antenna HSDPA scheme to explore future enhancements of the standard. To analyze the implementation loss, we introduce the so-called achievable mutual information and compare it with the actually measured data throughput. We find that the measured data throughput is far from the optimal, leaving room for future receiver optimizations. Furthermore, we find that the achievable mutual information is far from the channel capacity. Thus, optimizations in the standard could further improve HSDPA performance.**

***Index Terms*—Array signal processing, code-division multiple access, channel quality indicator (CQI), cross polarization, feedback communication, information rates, multiple-input–multiple-output (MIMO) systems, precoding control indicator (PCI), testbed measurements, throughput performance.**

I. Introduction

THE High-Speed Downlink Packet Access (HSDPA) mode [2] was introduced in Release 5 of the Universal Mobile Telecommunications System (UMTS) to provide high data rates to mobile users. Significant improvements are achieved by several techniques, such as fast link adaptation [3], fast hybrid automatic repeat request (HARQ) [4], and fast scheduling [5]. In contrast with the pure transmit power adaptation performed in former releases of UMTS, fast link adaptation in HSDPA adjusts the data rate and the number of spreading codes defined by the so-called channel quality indicator (CQI) feedback. Multiple-input–multiple-output (MIMO) HSDPA [6], which has recently been standardized in Release 7 of UMTS, further increases the maximum downlink data rate by spatially multiplexing two independently coded and modulated data streams. In addition, channel-adaptive spatial precoding is implemented at the base station. The standard defines a set of precoding vectors, one of which is chosen based on the so-called precoding control indicator (PCI) feedback obtained from the user equipment. To evaluate the performance of such a highly complex HSDPA system, researchers have chosen several different approaches.

A. Related Work

Most of the work published on HSDPA during recent years has concentrated on system-level simulations [7]–[15], in which an analytical model [16], [17] of the physical layer is employed. Other theoretical studies that entirely focus on simulations look into specific details of the HSDPA physical layer, e.g., HARQ [4], receive antenna diversity [18], equalizer architectures [19], [20], radio-frequency hardware impairments [21], or link adaptation [3]. A meaningful assessment of the performance, however, requires the evaluation of the complete physical layer rather than the evaluation of individual physical-layer parts. To the authors' knowledge, it is only in [22] that the throughput of a complete single-input–single-output (SISO) HSDPA system, including the link adaptation, was simulated and compared with the Shannon capacity of the additive white Gaussian noise (AWGN) channel. However, since HSDPA is typically operated in frequency-selective fading channels, the AWGN channel capacity is not a good performance bound, because it only considers the mean signal-to-noise ratio (SNR). A much better, more realistic, and tighter bound is obtained by calculating the channel capacity based on the channel realizations of the simulation.

Apart from simulations, HSDPA has been evaluated in a few experimental studies. In [23], the throughput performance of a SISO HSDPA system is simulated based on the so-called drive test measurements, which are used to collect the received pilot power strength along a specific route within a cell. In subsequent simulations, the authors of [23] utilize the pilot power strength to estimate the HSDPA throughput performance. An experimental evaluation of a MIMO HSDPA multiuser detector is provided in [24]. In this paper, the authors present the average throughput performance of different detectors at 30 indoor receiver locations. The impact of distributed antenna systems on the HSDPA performance in indoor environments is studied in [25]. The same authors performed extensive measurements with available SISO HSDPA hardware to develop guidelines for indoor HSDPA network planning and optimization in [26]. The quality of service in a live HSDPA network is investigated in [27]. Throughput measurement results of a SISO and a MIMO HSDPA system are presented in [28] and [29], respectively. Unfortunately, the results in [29] were obtained by employing only a nonstandard compliant MIMO scheme and are thus not

Manuscript received January 15, 2010; revised April 14, 2010 and June 25, 2010; accepted July 27, 2010. Date of publication August 16, 2010; date of current version November 12, 2010. This work was supported in part by the Christian Doppler Laboratory for Wireless Technologies for Sustainable Mobility, KATHREIN-Werke KG, and A1 Telekom Austria AG. The financial support by the Federal Ministry of Economy, Family and Youth and the National Foundation for Research, Technology and Development is gratefully acknowledged. This paper was presented in part at the 70th IEEE Vehicular Technology Conference, Anchorage, AK, Sept. 2009. The review of this paper was coordinated by Prof. H. Liu.

The authors are with the Institute of Communications and Radio-Frequency Engineering, Vienna University of Technology, 1040 Vienna, Austria.

Color versions of one or more of the figures in this paper are available online at http://ieeexplore.ieee.org.

Digital Object Identifier 10.1109/TVT.2010.2066996

representative of next-generation HSDPA systems. In addition, none of the aforementioned papers compares the actual data throughput of a standard compliant MIMO HSDPA system with the mutual information and/or the capacity of the wireless channel. Thus, it cannot be inferred from previous publications how far HSDPA operates from the channel capacity. Furthermore, previous publications typically do not employ a systematic averaging approach, and thus, a mean scenario performance cannot be determined, with the result that such measurements are not repeatable.

B. Contribution

We performed physical-layer MIMO HSDPA throughput measurements. The main contributions of this paper are listed as follows.

1) Results obtained in two extensive measurement campaigns are presented. One campaign took place in an alpine valley in Austria. In this valley, the propagation channel had a relatively small mean root-mean-square (RMS) delay spread[1] of approximately 1 chip (260 ns), because relevant scattering objects existed only in the immediate vicinity of the receiver. The second campaign was carried out in the inner city of Vienna, Austria. In the city, the propagation conditions were non–line of sight, with a rather large mean RMS delay spread of approximately 4.3 chips (1.1 μs). In both scenarios, the receiver is static during a measurement; i.e., its channel does not change during the reception of one subframe.
2) In all measurements, cross-polarized antennas were utilized at the transmitter and receiver sites. This case is in contrast to simulations, in which only channel models with a single polarization are usually employed (see the detailed discussion as follows).
3) The 1×1, 1×2, 2×1, and 2×2 HSDPA schemes are implemented fully standard compliant. Thus, the results presented in this paper can be used to predict the potential benefits of employing MIMO in existing SISO HSDPA networks.
4) In addition to the already-standardized HSDPA schemes (up to 2×2 MIMO), an advanced four-transmit-antenna HSDPA scheme was defined and measured to explore future enhancements of the standard.
5) The throughput measurement results are compared to the so-called achievable mutual information, which is calculated based on the mutual information of the channel and the restrictions of the HSDPA standard. This comparison offers detailed insight into the implementation losses of the receiver, as explained in Section V-C.

As opposed to the simulations, we plot our measurement results over transmit power. This approach is necessary because of two reasons. First, the adaptive precoding employed in Release 7 of HSDPA very strongly influences the receiver SNR while leaving the sum transmit power unchanged. Plotting over the receive SNR would thus shift the throughput curves of the different HSDPA schemes against each other. Second, we typically observe large deviations in the average receive SNR of 3–5 dB between different receive antennas, although they are only spaced half a wavelength apart. Typically, such deviations are not reflected by channel models that offer identical average receive SNR for each receive antenna. Identical average receive SNRs would only be obtained in a very symmetrical transmission system, in which scattering objects are homogenously distributed around the antennas. Nevertheless, to facilitate comparisons of our measurement results with simulation results, we compute and display the average SISO receive SNR and the average SISO receive power in the result figures.

[1]The mean RMS delay spread was calculated by averaging the RMS delay spreads of all channel realizations (measurement positions).

C. Measurements Versus Simulations

Ideally, the performance of communication systems such as HSDPA should be evaluated for general wireless channels. This requirement is typically accomplished by two approaches: 1) simulation and 2) measurement. Both approaches have their individual pros and cons, which are briefly discussed as follows.

Simulations always rely on models of wireless channels and do not (at least not directly) require costly measurement campaigns. To obtain reasonable simulation results, realistic channel models have to be employed. In general, such models are highly complex and have many parameters that have to carefully be set to meaningful values. One very recent example is the Winner Phase 2+ channel model [30]. It includes almost all known physical wave propagation effects. However, two significant effects that are currently (July 2010) not well modeled are antenna polarization effects and multiuser correlation. The problem of these (and, possibly, also other currently unknown) missing physical effects in channel models can be circumvented by performing measurements. By performing measurements, all physical effects, whether known or unknown, (well) modeled or not, are included, thus achieving realistic results. By choosing setups that network providers have chosen (nearby existing base stations), we ensured that the selected scenarios are typical and the results obtained are meaningful. Our measurement results include antenna polarization effects and, possibly, numerous other effects that are currently not known and thus also not modeled.

In simulations, however, we have to first know all physical effects and, in the second step, to accurately model them. Both steps are difficult to carry out, and no current model can guarantee this condition. Performing measurements is thus a method for obtaining realistic results with correct quantitative measures. The conclusions drawn from measurements can directly be applied to modify systems, whereas the conclusions from simulations depend on the details of the model and how the numerous model parameters were selected. However, measurements are much more time and cost intensive than simulations and can therefore only be performed in a limited number of scenarios. Thus, measurements are ideally suited as a supplement to simulations and, in particular, to obtain quantitative results.

This paper is organized as follows. In Section II, we provide an introduction to MIMO HSDPA and then explain transmit precoding and receiver processing. Section III explains our measurement setup and methodology. The term *achievable*

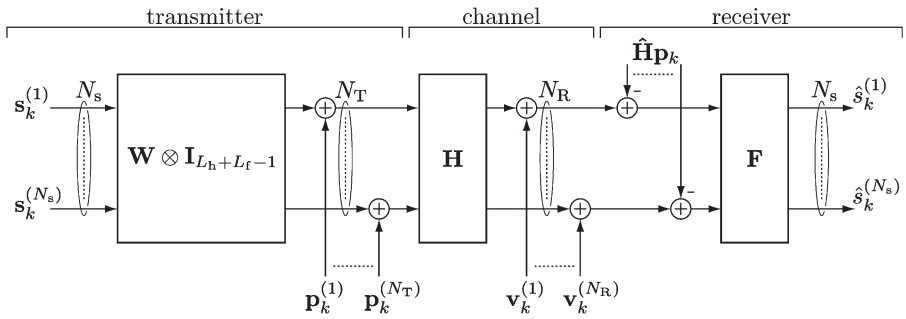

Fig. 1. Generalized system model of the HSDPA physical layer.

mutual information is introduced in Section IV as a performance bound for the measured throughput. Furthermore, we define in Section IV several novel loss metrics. The measurement results are presented in Section V. We conclude this paper in Section VI.

II. Multiple-Input–Multiple-Output High-Speed Downlink Packet Access

In this section, we describe the MIMO HSDPA physical layer. In particular, we elaborate on the precoding at the transmitter, the mathematical representation of the channel, and the equalization at the receiver. The system model introduced describes a general MIMO HSDPA system and implies no restrictions on the maximum number of data streams, the number of antennas, and the precoding matrices. Only two restrictive assumptions are made in this section. First, we restrict our analysis to slow fading; i.e., we assume that the channel remains approximately constant during the transmission of one subframe (2 ms). Second, we assume that only one user per subframe is scheduled by the base station. This assumption is necessary because of the immense hardware effort required for multiuser measurements. It should also be noted that multiuser scheduling for HSDPA is currently a topic of research [31]–[33] and it remains an open question how such scheduling can optimally be implemented.

In the following three sections, we define the mathematical system model, the receiver, and the quantized precoding of HSDPA.

A. System Model

Assume the spatially multiplexed transmission of N_s independently coded and modulated data chip streams, each of length $L_\mathrm{c} = L_\mathrm{h} + L_\mathrm{f} - 1$ chips, where L_h and L_f correspond to the channel and the equalizer length, respectively. A block diagram of this transmission system is shown in Fig. 1. We define the stacked transmit chip vector $\mathbf{s}_k$ of length $N_\mathrm{s}L_\mathrm{c}$ at time instant k as

$$\mathbf{s}_k = \left[\mathbf{s}_k^{(1)\mathrm{T}}, \ldots, \mathbf{s}_k^{(N_\mathrm{s})\mathrm{T}}\right]^\mathrm{T}. \tag{1}$$

The N_s chip streams are weighted by the $N_\mathrm{T} \times N_\mathrm{s}$-dimensional precoding matrix

$$\mathbf{W} = \begin{bmatrix} w^{(1,1)} & \cdots & w^{(1,N_\mathrm{s})} \\ \vdots & \ddots & \vdots \\ w^{(N_\mathrm{T},1)} & \cdots & w^{(N_\mathrm{T},N_\mathrm{s})} \end{bmatrix} \tag{2}$$

that forms the data chip streams of the N_T transmit antennas. At each transmit antenna, pilot, synchronization, and control channels accumulated in

$$\mathbf{p}_k = \left[\mathbf{p}_k^{(1)\mathrm{T}}, \ldots, \mathbf{p}_k^{(N_\mathrm{T})\mathrm{T}}\right]^\mathrm{T} \tag{3}$$

are added. Using the identity matrix $\mathbf{I}_{L_\mathrm{c}}$ of dimension $L_\mathrm{c} \times L_\mathrm{c}$, the transmit signal vector $\mathbf{a}_k$ of length $N_\mathrm{T}L_\mathrm{c}$ at time instant k is given by

$$\mathbf{a}_k = (\mathbf{W} \otimes \mathbf{I}_{L_\mathrm{c}})\mathbf{s}_k + \mathbf{p}_k. \tag{4}$$

The frequency-selective link between the n_tth transmit and the n_rth receive antenna is modeled by the $L_\mathrm{f} \times L_\mathrm{c}$-dimensional band matrix

$$\mathbf{H}^{(n_\mathrm{r},n_\mathrm{t})} = \begin{bmatrix} h_0^{(n_\mathrm{r},n_\mathrm{t})} & \cdots & h_{L_\mathrm{h}-1}^{(n_\mathrm{r},n_\mathrm{t})} & 0 \\ \ddots & & \ddots & \\ 0 & h_0^{(n_\mathrm{r},n_\mathrm{t})} & \cdots & h_{L_\mathrm{h}-1}^{(n_\mathrm{r},n_\mathrm{t})} \end{bmatrix} \tag{5}$$

in which $h_i^{(n_\mathrm{r},n_\mathrm{t})}$ $(i = 0, \ldots, L_\mathrm{h} - 1)$ represent the channel impulse response between the n_tth transmit antenna and the n_rth receive antenna. The entire frequency-selective MIMO channel is modeled by the following block matrix $\mathbf{H}$, which consists of $N_\mathrm{R} \times N_\mathrm{T}$ band matrices as defined in (5):

$$\mathbf{H} = \begin{bmatrix} \mathbf{H}^{(1,1)} & \cdots & \mathbf{H}^{(1,N_\mathrm{T})} \\ \vdots & \ddots & \vdots \\ \mathbf{H}^{(N_\mathrm{R},1)} & \cdots & \mathbf{H}^{(N_\mathrm{R},N_\mathrm{T})} \end{bmatrix}. \tag{6}$$

At the receiver input, the sum of noise and out-of-cell interference, which is denoted by $\mathbf{v}_k$, deteriorates the desired signal, i.e.,

$$\mathbf{b}_k = \mathbf{H}\mathbf{a}_k + \mathbf{v}_k = \mathbf{H}(\mathbf{W} \otimes \mathbf{I}_{L_\mathrm{c}})\mathbf{s}_k + \mathbf{H}\mathbf{p}_k + \mathbf{v}_k. \tag{7}$$

B. Receiver

At the receiver, we first perform synchronization and iterative channel estimation (three iterations) according to [34]. The interference of the deterministic signals, i.e., the pilot and the synchronization channels (SCHs), is then canceled. Therefore, in (7), the term $\mathbf{H}\mathbf{p}_k$ is reduced by $\hat{\mathbf{H}}\mathbf{p}_k$. The remaining interference is only caused by the channel estimation error $\mathbf{H} - \hat{\mathbf{H}}$ and the data channels [35]. Without this interference cancelation, the postequalization signal-to-interference-plus-noise ratio (SINR) would saturate at approximately 20 dB. Thus, CQI values that require higher SINR cannot be selected,

leading to a saturation of the throughput [36]–[38]. Alternatively to interference cancelation, interference-aware equalization is possible and was shown to achieve high performance [39]–[41].

The receive signal after interference cancelation, defined as $\mathbf{b}_k - \hat{\mathbf{H}}\mathbf{p}_k$, is processed in an equalizer $\mathbf{F}$ to obtain an estimate of the transmitted chip stream, i.e.,

$$\begin{aligned}\hat{\mathbf{s}}_k &= \left[\hat{s}_{k-\tau}^{(1)}, \ldots, \hat{s}_{k-\tau}^{(N_\mathrm{s})}\right]^\mathrm{T} = \mathbf{F}(\mathbf{b}_k - \hat{\mathbf{H}}\mathbf{p}_k) \\ &= \mathbf{F}\mathbf{H}(\mathbf{W} \otimes \mathbf{I}_{L_\mathrm{c}})\mathbf{s}_k + \underbrace{\mathbf{F}(\mathbf{H} - \hat{\mathbf{H}})\mathbf{p}_k}_{\approx \mathbf{0}} + \mathbf{F}\mathbf{v}_k. \end{aligned} \tag{8}$$

The equalizer matrix $\mathbf{F}$ consists of N_s vectors, each of length $N_\mathrm{R}L_\mathrm{f}$, and is composed as

$$\mathbf{F} = \left[\mathbf{f}^{(1)}, \ldots, \mathbf{f}^{(N_\mathrm{s})}\right]^\mathrm{T}. \tag{9}$$

In this paper, we calculate the equalizer coefficients in the minimum mean-square-error sense. Thus, for the equalizer of the n_sth data stream, we obtain

$$\begin{aligned}\mathbf{f}^{(n_\mathrm{s})} = &\left(\mathbf{H}\left(\mathbf{W}\mathbf{W}^\mathrm{H} \otimes \mathbf{I}_{L_\mathrm{c}}\right)\mathbf{H}^\mathrm{H} + \sigma_v^2 \mathbf{I}_{N_\mathrm{R}L_\mathrm{c}}\right)^{-1} \\ &\cdot \mathbf{H}(\mathbf{W} \otimes \mathbf{I}_{L_\mathrm{c}})\mathbf{e}_{\tau+(n_\mathrm{s}-1)L_\mathrm{c}}. \end{aligned} \tag{10}$$

The vector $\mathbf{e}_k$ denotes a unit vector with a single "one" at cursor position k and "zeros" at all other positions. The calculation of the equalizer coefficients can efficiently be implemented using fast Fourier transform (FFT)-based algorithms, e.g., [42] and [43], or the conjugated gradient algorithm [44]. Such an equalizer therefore represents a low-complexity HSDPA receiver that is feasible for real-time implementation in a chip [45]. The output of the equalizer is finally soft demapped and soft decoded in a turbo decoder using eight iterations. For completeness, we note that more complex MIMO receivers, such as the linear minimum mean-square-error maximum a posteriori (LMMSE-MAP), are known to show approximately 1 dB better performance than the straightforward LMMSE equalizer [46].

C. Quantized Precoding

In the HSDPA standard [2], the precoding matrix defined in Eq. (2) is strongly quantized and chosen from a predefined codebook. For single-antenna transmissions, in which no spatial precoding can obviously be performed, the precoding matrix $\mathbf{W}$ is reduced to a scalar equal to "one," i.e.,

$$\mathbf{W}^{(\mathrm{SISO})} = 1. \tag{11}$$

For multiple-antenna transmissions, the precoding matrices are composed of the scalars

$$w_0 = \frac{1}{\sqrt{2}} \tag{12}$$

$$w_1, w_2 \in \left\{\frac{1+\mathrm{j}}{2}, \frac{1-\mathrm{j}}{2}, \frac{-1+\mathrm{j}}{2}, \frac{-1-\mathrm{j}}{2}\right\}. \tag{13}$$

The transmit antenna array (TxAA) transmission mode utilizes two antennas to transmit a single stream. In this mode, the precoding matrix is defined as

$$\mathbf{W}^{(\mathrm{TxAA})} = \begin{bmatrix} w_0 \\ w_1 \end{bmatrix}. \tag{14}$$

This condition means that the signal at the first antenna is always weighted by the same scalar constant w_0, whereas the signal at the second antenna is weighted by w_1, which is chosen to maximize the received postequalization SINR [35]. In TxAA, the number of possible precoding matrices is equal to four, which corresponds to a feedback amount of 2 bit.

In the case of a double-transmit-antenna array (D-TxAA) transmission, the precoding matrix is given by

$$\mathbf{W}^{(\mathrm{D-TxAA})} = \begin{bmatrix} w_0 & w_0 \\ w_1 & -w_1 \end{bmatrix}. \tag{15}$$

Note that this precoding matrix is unitary, i.e., the precoding vector of the second stream is always chosen orthogonal to that of the first stream. Although D-TxAA defines four precoding matrices, only the first two matrices cause different SINRs at the receiver. In the other two cases, the SINRs of the first and second streams are exchanged. Because the data rates of both streams can individually be adjusted, the third and fourth precoding matrices are redundant. Note also that, if the user experiences low channel quality in D-TxAA, only a single stream is transmitted, i.e., the precoding matrix in (14) is applied to the data stream at the transmitter. Thus, in TxAA, a single stream is always transmitted, whereas in D-TxAA, either single- or double-stream transmission—whichever leads to a higher throughput—is performed.

The HSDPA standard does not define spatial precoding for four-transmit antennas. To explore the benefits of four-transmit antennas in HSDPA, a very simple extension of the existing precoding vectors is employed here. We define the precoding matrix for double-stream four-transmit antenna transmission as

$$\mathbf{W}^{(\mathrm{4Tx-D-TxAA})} = \begin{bmatrix} w_0 & 0 \\ 0 & w_0 \\ w_1 & 0 \\ 0 & w_2 \end{bmatrix}. \tag{16}$$

In contrast to the two-antenna D-TxAA system, the four-antenna D-TxAA system now transmits the two data streams on individual antenna pairs. In addition, the precoding of both streams is individually adjusted, allowing 16 possible precoding matrices.

III. Measurement Setup and Methodology

We now report on our MIMO HSDPA measurement setup in both alpine and urban scenarios.[2] Furthermore, we explain the feedback implementation and our averaging approach for obtaining the mean scenario performance. The measurement procedure utilizing our Vienna MIMO testbed [47] is explained in detail in [48].

[2]For both measured scenarios, detailed transmitter and receiver positions can be downloaded for Google Earth at http://www.nt.tuwien.ac.at/fileadmin/data/testbed/Vienna-and-Carinthia-TX-RX-GPS.kmz.

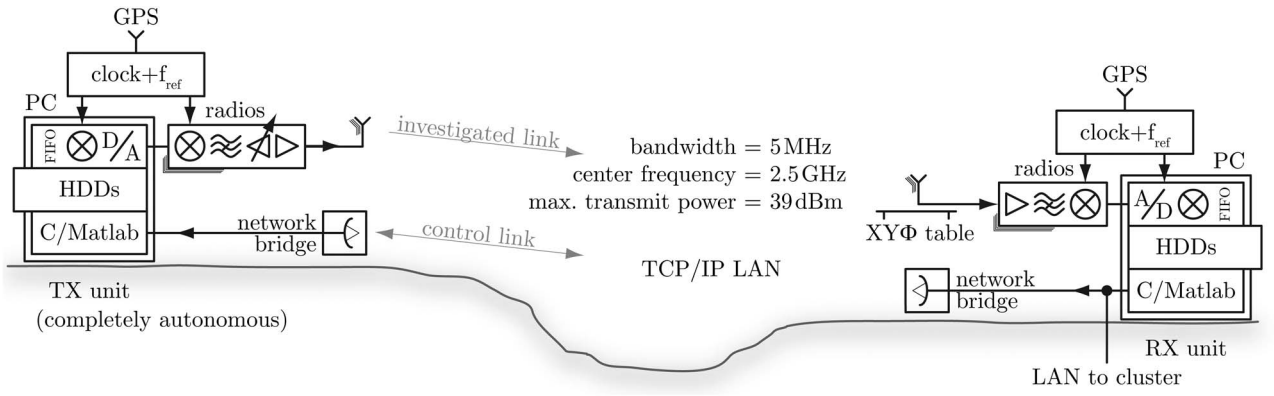

Fig. 2. Setup of the testbed in the alpine and urban scenarios.

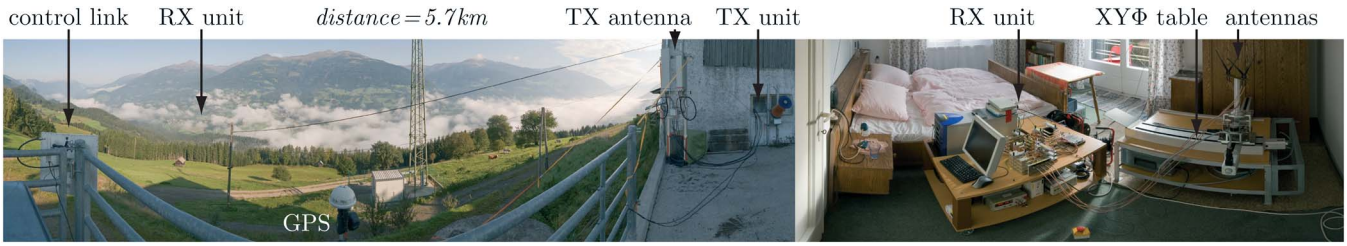

Fig. 3. Panoramic view of the alpine scenario measured (use PDF format to zoom).

Fig. 4. Panoramic view of the urban scenario measured (use PDF format to zoom).

A. Measurement Setup

Fig. 2 shows the basic measurement setup and important system parameters. This setup was employed in the following two scenarios.

- **Alpine scenario**. The XX-Pol base-station antenna (Kathrein 800 10629 [49], $2 \times \pm 45^\circ$ polarization, horizontal half-power beamwidth of 80°, vertical half-power beamwidth of 7.5°, down tilt of 6°, and 0.6 wavelength spacing between the cross-polarized elements) was placed at a distance of 5.7 km from the RX unit, which was located inside a house in a village on the opposite side of the Drau Valley, as shown in Fig. 3. The base-station antenna was mounted in a height of approximately 3 m above the ground, which corresponds to an effective height of approximately 300 m above the bottom of the Drau Valley. At the RX unit, we utilized standard Linksys WiFi-router rod antennas. The results presented in this paper were obtained in a setup in the alpine scenario, in which the receive antennas were placed indoors in non-line of sight to the transmitter. This setup is characterized by a short mean RMS delay spread of approximately 1 chip (260 ns) and one major propagation path, because the receive signal mainly propagates through a window that faces the transmit antennas. In addition to this setup, we investigated RX antenna positions in different rooms of the same house, where the TX antennas can and cannot be seen from the window. We also placed the RX unit outside, in the middle of a field, and with direct line of sight to the transmitter. In all the setups measured, the results obtained showed no significant change, except for a variation in the average path loss that only horizontally shifts the throughput curves measured.
- **Urban scenario**. The same base-station antenna as in the alpine scenario was placed on the roof of a tall building at the center of Vienna, Austria, at a distance of 430 m from the RX unit, which was placed inside an office (see Fig. 4). The base-station antenna was mounted in a height of approximately 3 m above the roof of the building, which corresponds to an effective height of approximately 45 m above street level. At the RX unit, we utilized four low-cost printed monopole antennas [50], which are based on the generalized Koch prefractal curve. Due to their low cost and small size, such antennas are very realistic and can be built into a mobile handset or a laptop computer. In all measurements carried out in the urban scenario, the

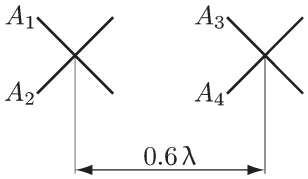

Fig. 5. Polarization and spatial separation of the TX antenna elements.

direct path from the TX to the RX antennas was blocked by the building in which the RX unit was located. This scenario is characterized by a rather large mean RMS delay spread of approximately 4.3 chips (1.1 μs).

In both scenarios, the TX antennas were placed adjacent to existing base-station antennas, making the selected base-station sites very realistic and representative of a mobile communication system. Note that no interference from the operational base-station antennas occurred during the measurement, because we used a carrier frequency of 2.5 GHz, which is different from the carrier frequencies of the mobile network providers in Austria, which operate around 2 GHz. The close carrier frequencies of the measurement and the mobile network ensure nearly identical behavior without impacting each other. We define the transmit power as the power measured at the output of the antenna feeder cable, i.e., the transmit power given in the figures in Section V is the power at the input of the Kathrein base-station antennas. By defining the transmit power this way, we compensate for the losses of the antenna feeder cables.

As aforementioned, the Kathrein 800 10629 base-station antenna [49] utilized in both the alpine and the urban scenarios, is a so-called XX-Pol antenna that consists of two antenna pairs (A_1, A_2) and (A_3, A_4). These two antenna pairs are cross polarized and spatially separated by 0.6 wavelengths (7 cm), as shown in Fig. 5. In the case of transmissions that required two transmitter outputs, one cross-polarized antenna pair (A_1, A_2) or (A_3, A_4) was utilized. When four-transmitter outputs were required, the first spatial data stream was transmitted with precoding on one polarization (A_1, A_3) and the second spatial data stream on the other polarization (A_2, A_4). In other words, each data stream was transmitted on the two equally polarized antennas, separated by 0.6 wavelengths: either (A_1, A_3) or (A_2, A_4). Consequently, according to the definition of the precoding matrix in Section II-C, the first two transmitter outputs were connected to the first antenna pair (A_1, A_2), and the second two transmitter outputs were connected to the second antenna pair (A_3, A_4).

B. Feedback Implementation Based on Postequalization SINR

In HSDPA, the transmission is adapted to the current channel conditions. To obtain a realistic performance estimate, we therefore also have to carry out channel adaptation during the measurement. Based on the estimated channel coefficients and the estimated noise variance, the HSDPA feedback can be determined. This approach is accomplished by calculating the postequalization SINR for all possible precoding matrices (for both single- and double-stream transmissions, if applicable). All postequalization SINRs are then mapped to CQI values that correspond to transport block sizes that can be transmitted with a block error ratio (BLER) of less than 10%. The PCI value that corresponds to the precoding matrix that maximizes the transport block size is selected. The selected PCI value and the CQI value that corresponds to the maximized transport block size are fed back to the base station. By calculating the feedback this way, dynamic switching between single- and double-stream operations can be achieved, and the physical-layer data throughput is maximized. Note that, for our measurement, this feedback implementation implies that the single user in our experiment is always served with its maximum supported data rate. We therefore need to assume that the base station always has data that waits for transmission to the user. More details about the feedback calculation method, as well as analytical expressions for the postequalization SINR, can be found in [35].

The feedback calculation method employed in the measurements relies on an accurate estimation of the postequalization SINR, which was obtained using the analytical expressions in [35]. Thus, by comparing the estimated postequalization SINR to the observed postequalization SINR at the demapper output, we can verify our feedback calculation method. Such a comparison is shown on the left side of Fig. 6 for a simulation (ITU Pedestrian B channel model [51]) and on the right side of Fig. 6 for a measurement (alpine scenario). In the simulation, in which perfect channel knowledge is assumed at the receiver, the postequalization SINR increases almost linearly with the channel SNR. This result is in contrast to the measurement, in which the channel has to be estimated. As a consequence, the postequalization SINR saturates at higher channel SNRs. Fig. 6 shows that the estimated SINR is almost the same as the SINR observed at the demapper output, validating the feedback calculation method employed in the measurement campaign.

C. Measuring a Single HSDPA Subframe

To measure a single HSDPA subframe, we employ a closed-loop quasi-real-time testbed measurement approach, because the hardware and experience required is readily available [47], [48], [52], [53]. In short, this approach works as follows.

1) We create standard compliant transmit data blocks for all combinations of possible modulations, coding rates, and precoding matrices. These transmit data blocks are stored on flash disk drives with very low latency and high data transfer rate.
2) We read a single HSDPA transmit block from the flash drives to transmit it over the wireless channel.
3) We instantly calculate *only* the feedback that is mandatory for closed-loop HSDPA in MATLAB in approximately 40 ms (less than the channel coherence time).[3]
4) We send the feedback information to the transmitter using a wireless local area network bridge.
5) We read the channel adapted (already pregenerated) HSDPA transmit block from the flash drives to transmit it over the same wireless channel and store the received block on large hard disks.
6) We also transmit two possible retransmissions to store the received blocks on large hard disks. Note that, at

[3]Therefore, our measurement approach only works in quasistatic scenarios.

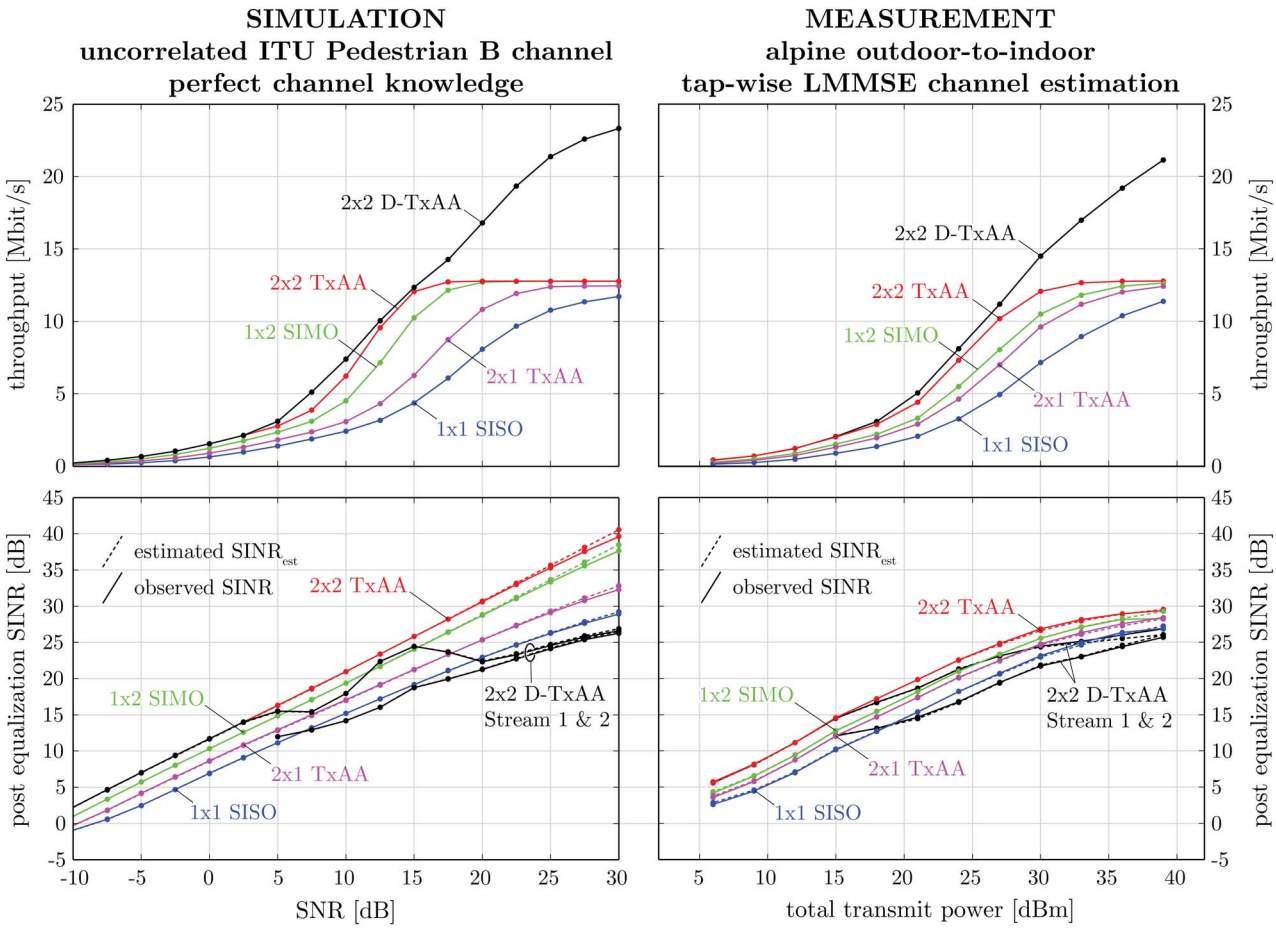

Fig. 6. Throughput and postequalization SINR: Simulation (Left), Measurement (Right) [35].

this stage, we still have not evaluated any received data blocks. Therefore, we currently cannot tell if a retransmission would be required, but still, we record it just in case it is needed.

7) Finally, after the measurement is completed, we evaluate the received data offline using a cluster of PCs. Results for the scenario measured are automatically obtained using the same program that has already controlled the complete measurement procedure and documentation (see [48] for a more detailed description).

D. Inferring Average Performance

The aim of this paper is to determine the throughput performance of the physical-layer link between a single base station and a single user. In reality, we are not interested in the performance at a specific channel realization (corresponding to fixed transmitter and receiver positions) but rather in the average performance, which could be, for example, the average performance that a user experiences when he randomly places his laptop computer on an office desk. In our measurements, we thus applied the averaging procedure explained as follows.

- We measure single HSDPA subframes (blocks) at different channel realizations (110 for the alpine scenario and 484 for the urban one). These realizations are created by moving the RX antennas with a fully automated XYΦ positioning table, as shown in Fig. 3. To minimize large-scale fading effects, we measure only within a small area of $3\lambda \times 3\lambda$. The measured antenna positions are uniformly distributed. By this systematic sampling approach, the distance between all positions measured is maximized, and their correlation is minimized.
- In the measurements, we observed a widely differing average path loss between the individual TX and RX antennas. This effect is shown in Fig. 7 in terms of the measured SISO throughput of all 16 individual links between the four TX antennas and the four RX antennas. At a throughput of 6 Mbit/s, the difference between the best and the worst SISO link is approximately 3.5 dB. Such a difference is in contrast with many channel models, which usually assume symmetric channels, i.e., the average performance of all SISO subchannels of a MIMO system is equal. The difference in average path loss can effectively be exploited by antenna selection algorithms, as we have demonstrated in [54]. However, in this paper, where the aim is to compare HSDPA schemes with different numbers of TX antennas, such an effect has to be compensated to obtain valid results. We achieve this aim by performing throughput averaging over the corresponding TX/RX antenna combinations. For example, if the 2×2 D-TxAA system is compared with the SISO transmission, the SISO throughput is obtained by averaging over the

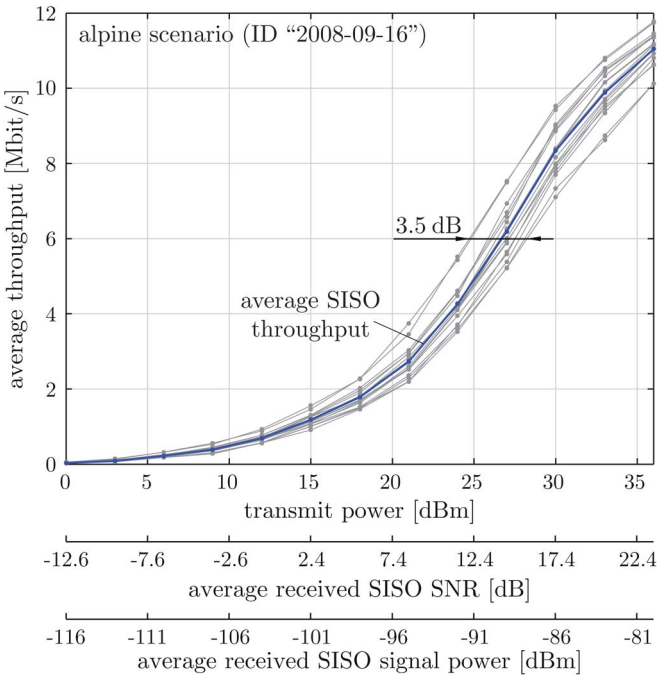

Fig. 7. SISO throughput of the 16 SISO subchannels of the 4 × 4 MIMO system in the alpine scenario (ID 2008-09-16).

four individual SISO links (TX1 → RX1, TX1 → RX2, TX2 → RX1, and TX2 → RX2).

To gauge the precision of the measured throughput, we utilize the BC_a bootstrap algorithm [55] to calculate the confidence intervals. In Fig. 8 in Section IV and Figs. 9–13 in Section V, the dots represent the average throughput values (rate values), the corresponding vertical lines represent the 95% confidence intervals, and the corresponding horizontal lines represent the 2.5% and 97.5% percentiles. Note that the RX antenna positions remained unchanged between measuring different schemes at different transmit power levels.

IV. Achievable Mutual Information

In this section, the so-called *achievable mutual information*[4] is defined. It is used as a feasible performance bound for the data throughput actually measured, given a specific standard (in this case, HSDPA Release 7). The calculation of the bound is based on the mutual information between transmit and receive signals. In particular, the achievable data throughput is a function of the wireless channel (i.e., the estimated frequency response and the noise variance) and the precoding vectors allowed by the standard. Thus, it incorporates the restrictions imposed by the transmission standard (quantized frequency-flat precoding) but not the restrictions imposed by the receiver employed.

For the calculation of the achievable mutual information, consider the estimated channel impulse response of length L_h

[4]Note that, in previous publications, we have used the term *achievable throughput* [1], [53], [56], but we are now convinced that the term *achievable mutual information* is much more suitable.

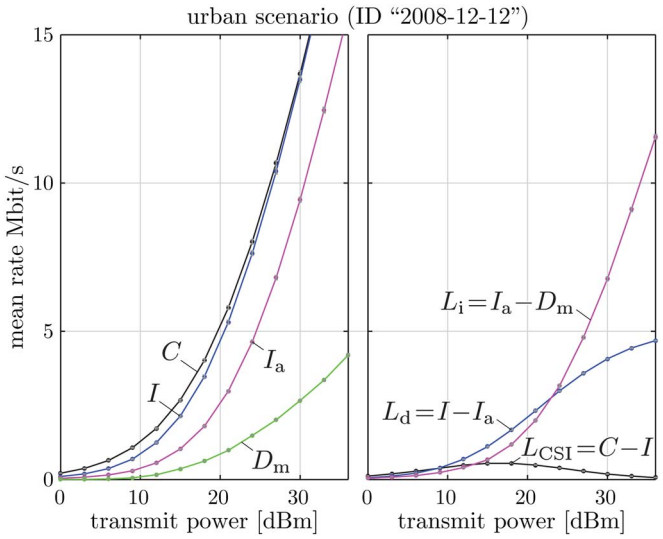

Fig. 8. Rates of the SISO system in the urban scenario (ID 2008-12-12). (Left) Channel capacity C, mutual information I, achievable mutual information I_a, and measured throughput D_m. (Right) CSI loss L_{CSI}, design loss L_d, and implementation loss L_i.

chips between the n_tth TX and the n_rth RX antennas, i.e.,

$$\hat{\mathbf{h}}^{(n_r,n_t)} = \left[\hat{h}_0^{(n_r,n_t)} \quad \dots \quad \hat{h}_{L_h-1}^{(n_r,n_t)}\right]^T. \tag{17}$$

Note that the channel coefficients in this vector depend on the RX antenna position and the transmit power, as do all the terms defined as follows. The channel vector $\hat{\mathbf{h}}^{(n_r,n_t)}$ can equivalently be described in the frequency domain as $\hat{\mathbf{g}}^{(n_r,n_t)} = \mathfrak{F}\{\hat{\mathbf{h}}^{(n_r,n_t)}\}$ by using the N_{FFT}-point Fourier transform $\mathfrak{F}\{.\}$. Thus, the Fourier transform separates the frequency-selective channel into N_{FFT} frequency-flat channels. Using the notation $(.)_m$ to extract the mth element of a vector, the estimated $N_R \times N_T$ MIMO channel matrix of the mth $(m = 1, \dots, N_{FFT})$ frequency bin can then be written as

$$\hat{\mathbf{G}}_m = \begin{bmatrix} \left(\hat{\mathbf{g}}^{(1,1)}\right)_m & \dots & \left(\hat{\mathbf{g}}^{(1,N_T)}\right)_m \\ \vdots & \ddots & \vdots \\ \left(\hat{\mathbf{g}}^{(N_R,1)}\right)_m & \dots & \left(\hat{\mathbf{g}}^{(N_R,N_T)}\right)_m \end{bmatrix}. \tag{18}$$

By using the well-known expressions for the MIMO capacity (for example, see [57] and [58]), we obtain the achievable mutual information for the measured channel $\hat{\mathbf{G}}_m$ as

$$I_a = \max_{\mathbf{W}\in\mathcal{W}} \sum_{m=1}^{N_{FFT}} \frac{f_s}{N_{FFT}} \log_2 \det\left(\mathbf{I}_{N_R} + \frac{1}{\sigma_v^2}\hat{\mathbf{G}}_m \mathbf{W}\mathbf{W}^H \hat{\mathbf{G}}_m^H\right). \tag{19}$$

Here, σ_v^2 is the variance of the noise $\mathbf{v}_k$, and $f_s = 3.84$ MHz is the equivalent rectangular bandwidth of the root raised cosine (RRC) filtered HSDPA signal. The maximization in (19) is performed over the set $\mathcal{W}$ of all possible precoding matrices. A few remarks should be made about the definition of the achievable mutual information as follows.

1) The channel coefficients in (19) are the channel coefficients of the data channel that is transmitted at a specific portion (in our case, −4 dB) of the base station's

TABLE I
MEASUREMENT PARAMETERS

	Alpine Scenario	Urban Scenario
User equipment category	16	16
HS-PDSCH E_c/I_{or}	-4 dB	-4 dB
CPICH E_c/I_{or}	-10 dB	-10 dB
SCH/PCCPCH E_c/I_{or}	-12 dB	-12 dB
E_c/I_{or} of other channels	-3.6 dB	-3.6 dB
Channel estimator length L_h	23 chips	48 chips
Equalizer length L_f	30 chips	60 chips

total transmit power. The remaining power is required for the transmission of the nondata channels, i.e., the transmission of the pilot, control, and SCHs. By proper scaling of the channel coefficients in (19), the inherent loss in spectral efficiency caused by the transmission of the nondata channels is automatically included in the achievable mutual information.

2) Equation (19) represents neither the mutual information (obtained without precoding) nor the channel capacity (obtained by optimal water filling), because quantized and frequency-flat precoding is utilized in HSDPA. Therefore, we have introduced the new term *achievable mutual information* for the symbol I_a.
3) Equation (19) only gives the achievable mutual information for a specific channel realization at a specific RX antenna position and at a given transmit power level. To obtain the mean achievable mutual information, we perform averaging over all measured RX antenna positions.
4) To increase the accuracy of the estimated channel coefficients in (19), we utilize the channel coefficients at the largest transmit power to calculate the achievable mutual information. At lower transmit powers, the different channel SNRs are obtained by scaling the channel coefficients accordingly.

Alternatively to the achievable mutual information, the well-known *channel capacity* C, requiring that full channel-state information (CSI) is available at the transmitter side, and the *mutual information* I, can be used as performance bounds. For the case of a SISO transmission in the urban scenario, Fig. 8 visualizes these three performance bounds, the *measured data throughput* D_m, and the relations between them. In this scenario, the channel capacity C, which could theoretically be achieved if optimum water filling [59], [60] is employed at the transmitter side, is slightly greater than the mutual information I. In the case of SISO transmission, the achievable mutual information is the same as the mutual information, shifted by 4 dB in transmit power, because in our measurement, the data channel high-speed physical-downlink shared channel (HS-PDSCH) is transmitted at an offset of -4 dB against the total transmit power (see Table I). Note that, for any other choice of power offset, the achievable mutual information curve would shift accordingly.

The right side of Fig. 8 shows three losses [61], which we define as follows.

- For the *CSI loss*, we have

$$L_{CSI} = C - I \tag{20}$$

which refers to the difference between the channel capacity C and the mutual information I. It accounts for a missing full CSI at the transmitter side. An ideal transmission system without available CSI at the transmitter can only achieve a rate equal to the mutual information. Compared with the other two losses defined as follows, the CSI loss is almost negligible, particularly at higher transmit powers and, thus, higher SNRs [62].

- For the *design loss*, we have

$$L_d = I - I_a \tag{21}$$

which refers to the difference between the mutual information I and the achievable mutual information I_a. It accounts for inherent system design losses caused by, for example, the necessary transmission of pilot symbols. In the medium transmit power range of 10–20 dBm, the design loss causes most of the overall system losses.

- For the *implementation loss*, we have

$$L_i = I_a - D_m \tag{22}$$

which refers to the difference between the achievable mutual information I_a and the measured data throughput D_m. It accounts for losses caused by nonoptimum receivers and channel codes. At higher transmit powers, the implementation loss becomes dominant. A more detailed discussion of the individual parts of the implementation loss is provided in Section V-C.

V. MEASUREMENT RESULTS

In this section, the throughput measurement results (the solid lines in Figs. 9–12) are presented and compared with the achievable mutual information (the dashed lines in Figs. 9–12). The most important HSDPA parameters are listed in Table I. The E_c/I_{or} values indicate how much of the total transmit power is allocated for the transmission of HS-PDSCH, the common pilot channel (CPICH), the synchronization channel (SCH), and the primary common control physical channel (PCCPCH). Note that, in a real network, many more physical channels would be transmitted by the base station than we did in our experiments. For example, a base station needs to transmit the paging indication channels to support UMTS voice calls. Although we do not actually transmit these channels in our experiment, we have to consider their portion of the total transmit power to realistically assess the performance losses of HSDPA (as done, for example, in Fig. 8). We reserve -3.6 dB of the base station's total transmit power for these channels in our budget.

The user equipment category in Table I defines the maximum supported data rate. In our experiment, in which we utilize the CQI mapping table of a category-16 user equipment, the maximum data rate in the single-stream mode is 12.779 Mbit/s, and in the double-stream mode, the maximum data rate is 27.952 Mbit/s.

In the figures, all throughput curves are plotted over the transmit power. Two additional abscissas show the average (over all channel realizations and all antennas) received SISO SNR and the average received SISO signal power. Note that

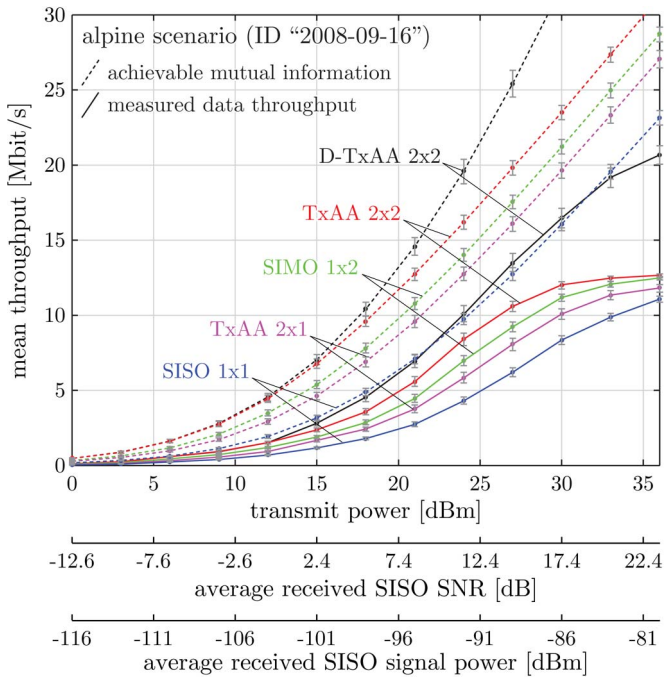

Fig. 9. Throughput results of the standard compliant schemes in the alpine scenario (ID 2008-09-16). Averaging was performed over 110 receiver positions.

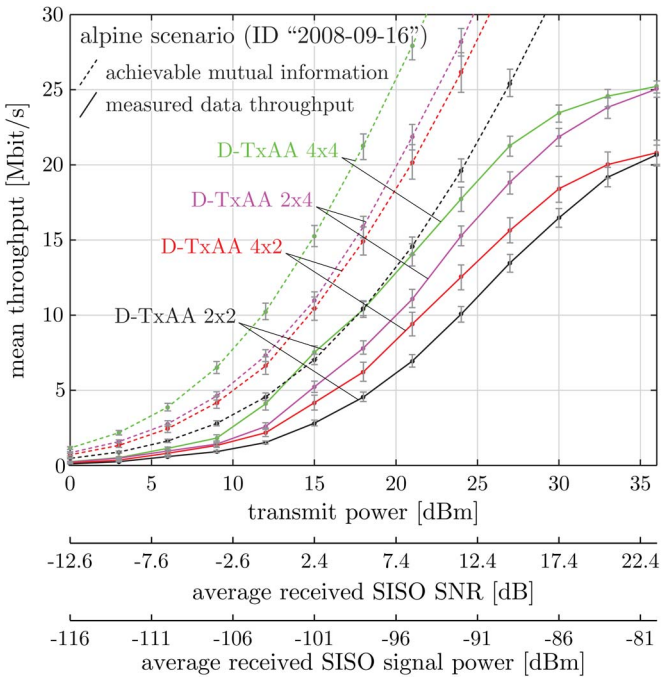

Fig. 10. Throughput results of the advanced schemes in the alpine scenario (ID 2008-09-16). Averaging was performed over 110 receiver positions.

the average SNR over all RX antennas does not necessarily reflect the typical SNR of an individual antenna, as explained in Section III-D.

The reason that the throughput is plotted over transmit power is given as follows. All MIMO schemes in HSDPA utilize adaptive precoding, which effectively increases the received power (and, thus, the SNR), whereas the total transmit power remains the same as in the SISO transmission. If the throughput is plotted over SNR rather than over transmit power, the curves will be shifted against each other. For example, in the case of TxAA, this shift would approximately be 2 dB compared with SISO. The additional abscissas (average received SISO SNR and average received SISO power) are thus only shown for reference to indicate the approximate SNR and receive power ranges.

A. Alpine Scenario

Fig. 9 shows the measured throughput and the achievable mutual information of the 1×1 SISO, the 1×2 single-input–multiple-output (SIMO), the 2×1 TxAA, the 2×2 TxAA, and the 2×2 D-TxAA transmission systems in the alpine scenario. Although all these schemes are standardized, to the authors' knowledge, only the 1×1 SISO transmission is currently used in HSDPA networks.

Several observations can be made with regard to Fig. 9.

- The measured throughput of the 2×1 TxAA system is significantly (approximately 3 dB) better than the throughput of the SISO system. The scalar precoding of the 2×1 TxAA system thus performs very well in this scenario, with low delay spread.
- The 2×2 D-TxAA system also performs very well, achieving more than twice the throughput of the SISO system. Compared with the 2×2 TxAA system, D-TxAA benefits from its optional second data stream, even at low transmit powers of approximately 15 dBm.
- The achievable mutual information of the 2×1 TxAA system is approximately 3 dB better than the SISO system. This result is in accordance with the measured data throughput curves, which also show a 3-dB performance increase for the 2×1 TxAA system.
- The achievable mutual information of the 2×2 D-TxAA system has a steeper slope than the 2×2 TxAA system. This result is caused by the inclusion of the quantized precoding matrices in the calculation of the achievable mutual information (see Section IV). In the case of the 2×2 TxAA system, the multiplication of the channel matrix with the precoding matrix effectively reduces the 2×2 system to a 1×2 system. In the case of the 2×2 D-TxAA system, the precoding matrix is unitary, maintaining the rank of the channel matrix. As a consequence of the higher channel rank, the achievable mutual information curve of the 2×2 D-TxAA system is steeper than the 2×2 TxAA system.

The comparison between the measured throughput and the achievable mutual information should be performed at a transmit power of approximately 10–25 dBm or a throughput of approximately 5 Mbit/s to avoid saturation effects of the measured throughput (because outside this range, neither smaller nor larger CQI values are available for channel adaptation). At large transmit power levels, when the single-stream transmission modes saturate, such a comparison would be unfair, because the throughput could easily be increased by providing additional modulation and coding schemes. At a throughput of 5 Mbit/s, the measured SISO and 2×2 D-TxAA throughputs lose approximately 7 and 6 dB, respectively, compared with their corresponding achievable mutual information.

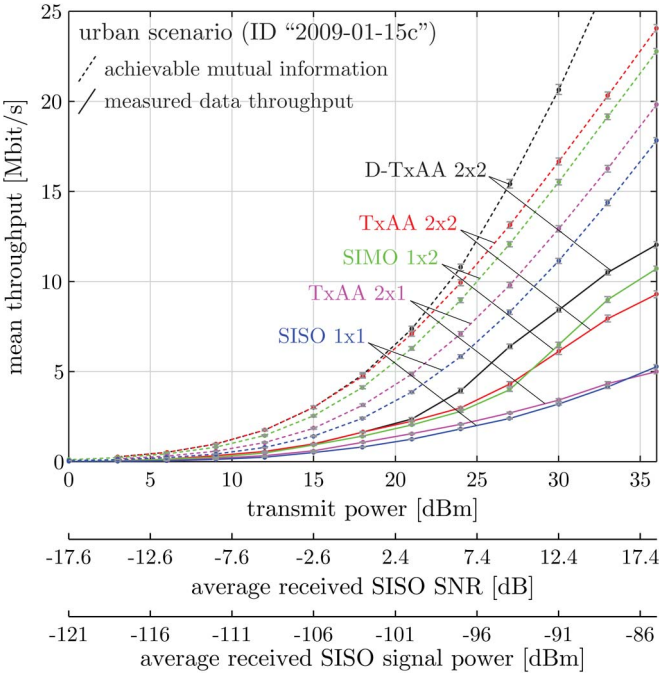

Fig. 11. Throughput results of the standard compliant schemes in the urban scenario (ID 2009-01-15c). Averaging was performed over 484 receiver positions.

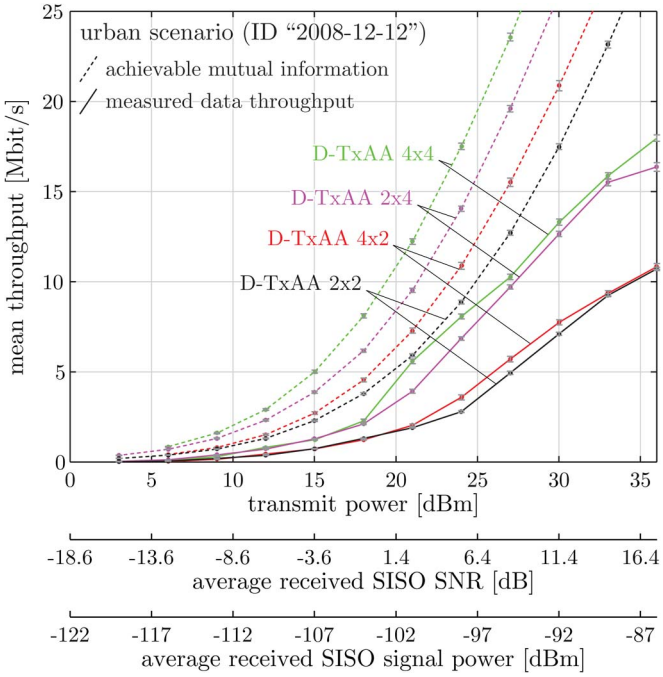

Fig. 12. Throughput results of the advanced schemes in the urban scenario (ID 2008-12-12). Averaging was performed over 484 receiver positions.

Fig. 10 shows the throughput of the four-transmit-antenna HSDPA schemes compared to the standard compliant 2×2 D-TxAA system in the alpine scenario. The following observations can be made.

- The measured throughput of the four-transmit-antenna schemes is significantly increased. For the 4×4 system, the measured throughput is approximately twice the 2×2 system. In terms of SNR, the 4×4 system gains approximately 6 dB compared with the 2×2 system.
- The theoretical maximum throughput of all four schemes, as shown in Fig. 10, is 27.952 Mbit/s. However, the measured throughput saturates before reaching this maximum value because of residual interference after the equalization. In the four-receive-antenna schemes, the equalizer can reduce the postequalization interference to a lower level than in the two-receive-antenna schemes. Therefore, the maximum measured data throughput of the four-receive-antenna schemes is greater than the two-receive-antenna schemes.
- A comparison of the achievable mutual information with the measured throughput reveals losses of approximately 6–7 dB for the schemes in Fig. 10.

B. Urban Scenario

In Fig. 11, the results of the standard compliant schemes in the urban scenario are shown. In contrast to the alpine scenario, at low SNRs, the 2×1 TxAA system only performs marginally better than the SISO system and is worse than SISO when the SNR is large. A similar observation can be made when comparing the throughput of the 2×2 TxAA system to the throughput of the 1×2 SIMO system in Fig. 11. Thus, it is not favorable to apply the standard compliant precoding of HSDPA in the urban scenario at high SNR. The reason for this surprising result is the rather large maximum delay spread of approximately 20 chips, which destroys the orthogonality of the spreading codes. As a consequence, the channel estimator performance suffers, because the pilots also experience high interference. In the case of transmissions with precoding, the channel estimator performance suffers even more, because the available pilot power is divided among the TX antennas, whereas the total data power, which acts as interference on the pilots, remains the same. The throughput degradation measured is explained by the fact that, at high SNR, the HSDPA performance mainly depends on the channel estimator performance [35].

Comparing the measured data throughput with the achievable mutual information yields approximately 9 dB loss in terms of SNR for the SISO system, which is approximately 3 dB more than the alpine scenario. As in the alpine scenario, the 2×2 D-TxAA system yields approximately twice the throughput of the SISO system.

The results for the four-transmit-antenna schemes in the urban scenario are plotted in Fig. 12. Here, the gains of the four-transmit-antenna schemes are approximately the same as in the alpine scenario. The 4×4 system outperforms the 2×2 system by slightly more than 6 dB in SNR or by more than a factor of two in terms of throughput. Fig. 12 also shows that, in the urban scenario, most of the throughput gains are due to the four RX antennas. Four transmit antennas only yield small throughput gains in this scenario.

C. Discussion of the Implementation Loss

Although the results of the previous sections show a significant increase in the performance of the different MIMO

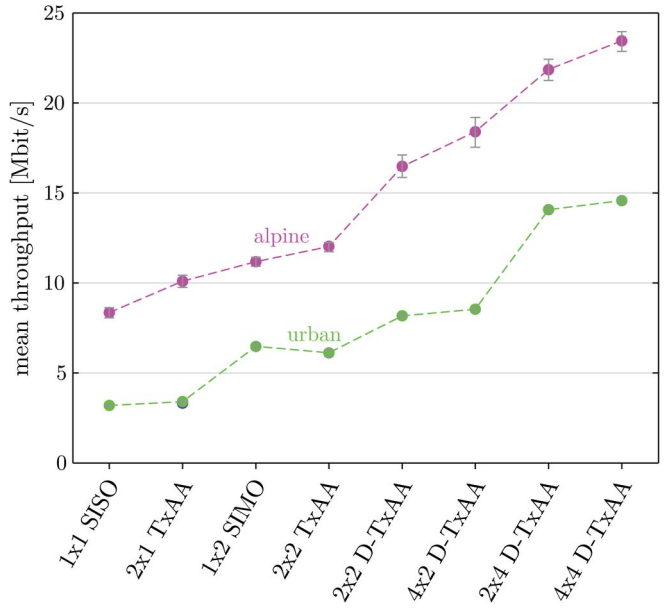

Fig. 13. Throughput of the different MIMO schemes in the alpine and the urban scenarios for transmit power $P_{\mathrm{TX}} = 30$ dBm.

schemes compared with the SISO transmission, all measured throughput curves are approximately 6–9 dB worse than the achievable mutual information. The following effects contribute (perhaps together with other possible causes) to this loss.

- The rate-matched turbo code utilized in HSDPA is good but not optimal. Our AWGN simulations show that, at higher code rates, it loses up to 2 dB when decoded by a max-log-MAP decoder *(approximately 2 dB)*.
- The LMMSE equalizer that represents a low-complexity and cost-effective solution is also not optimal. Better receivers such as the LMMSE-MAP have the potential to improve the performance by approximately 1 dB [46].
- In the urban scenario, a larger throughput loss was measured than in the alpine scenario because of the larger delay spread and, consequently, the larger intercode interference. For example, in the alpine scenario, the SISO system loses approximately 6 dB to the achievable mutual information, whereas the loss in the urban scenario is approximately 9 dB *(3 dB additional loss in the urban scenario compared to the alpine scenario)*.
- In addition to the aforementioned losses, channel estimation errors and overestimation/underestimation of the postequalization SINR degrade the measured throughput. Exactly quantifying the loss caused by these effects is difficult, because neither perfect CSI nor perfect postequalization SINR is available for measurement.

VI. Conclusion

MIMO HSDPA throughput measurement results obtained in two extensive measurement campaigns have been presented in this paper. The campaigns were carried out in an alpine valley in Austria and in the inner city of Vienna, Austria. The scenarios significantly differ in the delay spread of the channel. In both scenarios, the use of multiple antennas considerably increases the physical-layer throughput. The standard compliant 2×2 system increases the physical-layer throughput by more than a factor of two compared with the SISO system, whereas the 4×4 system further increases the throughput by a factor of two. Fig. 13 provides a comprehensive overview of the MIMO gains in HSDPA. In contrast with many channel models, we observe in the measurements a widely differing average path loss for the individual SISO subchannels of the MIMO system. We therefore had to apply throughput averaging to obtain a meaningful comparison between the HSDPA schemes with different numbers of antennas.

To compare the measured throughput to a performance bound, the achievable mutual information is defined. This achievable mutual information is calculated based on the mutual information of the channel and the precoding employed at the transmitter. Comparison of the measured throughput and the achievable mutual information shows that the measured throughput is far from the optimal, losing between 6 and 9 dB in the SNR. This loss is caused by the channel coding (approximately 2 dB), suboptimal LMMSE equalizer (approximately 1 dB), intercode interference (3 dB additional loss in the urban scenario compared to the alpine scenario), channel estimation errors, feedback errors (caused by overestimation/underestimation of the postequalization SINR), and, perhaps, other effects. Aside from this implementation loss, we define a design loss (mutual information minus the achievable mutual information) and a CSI loss (capacity minus mutual information). We find that the CSI loss is almost negligible throughout the SNR range. The design loss, however, is dominant in the medium transmit power range, which corresponds to a receive SNR of approximately 0 dB.

Acknowledgment

The authors would like to thank C. Kakoyiannis of the National Technical University of Athens, Greece, for providing the printed monopole RX antennas utilized in the measurements, KATHREIN-Werke KG for providing the TX antennas, and J. A. García Naya, M. Šimko, W. Schüttengruber, C. F. Mecklenbräuker, and G. Maier for their support in setting up the testbed.

References

[1] C. Mehlführer, S. Caban, and M. Rupp, "MIMO HSDPA throughput measurement results in an urban scenario," in *Proc. 70th IEEE VTC–Fall*, Anchorage, AK, Sep. 2009, pp. 1–5. [Online]. Available: http://publik.tuwien.ac.at/files/PubDat_176321.pdf

[2] 3GPP, Technical Specification Group Radio Access Network: Physical Layer Procedures (FDD) (3GPP TS 25.214 v7.7.0), Nov. 2007. [Online]. Available: http://www.3gpp.org/ftp/Specs/html-info/25214.htm

[3] M. Nakamura, Y. Awad, and S. Vadgama, "Adaptive control of link adaptation for high-speed downlink packet access (HSDPA) in WCDMA," in *Proc. 5th IEEE Int. Symp. Wireless Pers. Multimedia Commun.*, Oct. 2002, vol. 2, pp. 382–386. [Online]. Available: http://ieeexplore.ieee.org/stamp/stamp.jsp?arnumber=1088198

[4] A. Das, F. Khan, A. Sampath, and H.-J. Su, "Performance of hybrid ARQ for high-speed downlink packet access in UMTS," in *Proc. 54th IEEE VTC–Fall*, 2001, vol. 4, pp. 2133–2137. [Online]. Available: http://ieeexplore.ieee.org/stamp/stamp.jsp?arnumber=957121

[5] H. N. Nguyen, R. Esmailzadeh, and I. Sasase, "A fast scheduling algorithm considering buffer occupancy and channel condition for High-Speed Downlink Packet Access," in *Proc. 6th Int. Symp. WPMC*, Oct. 2003, pp. 72–76. [Online]. Available: http://www.sasase.ics.keio.ac.jp/pdf/55745wpmc_nguyen.pdf

[6] H. Holma, A. Toskala, K. Ranta-aho, and J. Pirskanen (2007, Dec.), High-speed packet access evolution in 3GPP release 7. *IEEE Commun. Mag.* [Online]. *45(12)*, pp. 29-35. Available: http://ieeexplore.ieee.org/stamp/stamp.jsp?arnumber=4395362

[7] T. E. Kolding, K. I. Pedersen, J. Wigard, F. Frederiksen, and P. E. Mogensen (2003, Feb.), High-speed downlink packet access: WCDMA evolution. *IEEE Veh. Technol. Soc. News*. [Online]. vol. 50, no. 1, pp. 4-10. Available: http://kom.aau.dk/group/05gr943/literature/hsdpa/evolution%20of%20HSDA.pdf

[8] S. Parkvall, E. Dahlman, P. Frenger, P. Beming, and M. Persson, "The evolution of WCDMA towards higher speed downlink packet data access," in *Proc. 53rd IEEE VTC–Spring*, 2001, vol. 3, pp. 2287–2291. [Online]. Available: http://ieeexplore.ieee.org/stamp/stamp.jsp?arnumber=945103

[9] S. Parkvall, E. Dahlman, P. Frenger, P. Beming, and M. Persson, "The high-speed packet data evolution of WCDMA," in *Proc. 12th IEEE Int. Symp. PIMRC*, Sep. 2001, vol. 2, pp. G-27–G-31. [Online]. Available: http://ieeexplore.ieee.org/stamp/stamp.jsp?arnumber=965315

[10] T. Moulsley, "Throughput of high-speed downlink packet access for UMTS," in *Proc. 2nd IEEE Int. Conf. 3G Mobile Commun. Technol. (3G)*, 2001, pp. 363–367. [Online]. Available: http://ieeexplore.ieee.org/stamp/stamp.jsp?arnumber=923569

[11] T. Kolding, F. Frederiksen, and P. Mogensen, "Performance aspects of WCDMA systems with high-speed downlink packet access (HSDPA)," in *Proc. 56th IEEE VTC–Fall*, 2002, vol. 1, pp. 477–481. [Online]. Available: http://ieeexplore.ieee.org/stamp/stamp.jsp?arnumber=1040389

[12] R. Love, A. Ghosh, R. Nikides, L. Jalloul, M. Cudak, and B. Classon, "High-speed downlink packet access performance," in *Proc. 53rd IEEE VTC–Spring*, 2001, vol. 3, pp. 2234–2238. [Online]. Available: http://ieeexplore.ieee.org/stamp/stamp.jsp?arnumber=945093

[13] R. Love, A. Ghosh, W. Xiao, and R. Ratasuk, "Performance of 3GPP high-speed downlink packet access (HSDPA)," in *Proc. IEEE 60th VTC–Fall*, Sep. 2004, vol. 5, pp. 3359–3363. [Online]. Available: http://ieeexplore.ieee.org/stamp/stamp.jsp?tp=&arnumber=1404686

[14] K. Pedersen, T. Lootsma, M. Stttrup, F. Frederiksen, T. Kolding, and P. Mogensen, "Network performance of mixed traffic on high-speed downlink packet access and dedicated channels in WCDMA," in *Proc. IEEE 60th VTC–Fall*, Sep. 2004, vol. 6, pp. 4496–4500. [Online]. Available: http://ieeexplore.ieee.org/stamp/stamp.jsp?tp=&arnumber=1404930

[15] I. Siomina and D. Yuan, "Enhancing HSDPA performance via automated and large-scale optimization of radio base station antenna configuration," in *Proc. 67th IEEE VTC–Spring*, May 2008, pp. 2061–2065. [Online]. Available: http://ieeexplore.ieee.org/stamp/stamp.jsp?tp=&arnumber=4526019

[16] M. Assaad and D. Zeghlache, "On the capacity of HSDPA," in *Proc. 46th IEEE GLOBECOM*, Dec. 2003, vol. 1, pp. 60–64. [Online]. Available: http://ieeexplore.ieee.org/stamp/stamp.jsp?arnumber=1258203

[17] M. Assaad and D. Zeghlache, "Comparison between MIMO techniques in UMTS–HSDPA system," in *Proc. 8th IEEE Int. Symp. Spread Spectrum Tech. Appl.*, Aug. 2004, pp. 874–878. [Online]. Available: http://ieeexplore.ieee.org/stamp/stamp.jsp?arnumber=1371826

[18] J. Kunze, C. Schmits, A. Bilgic, and J. Hausner, "Receive antenna diversity architectures for HSDPA," in *Proc. 67th IEEE VTC–Spring*, May 2008, pp. 2071–2075. [Online]. Available: http://ieeexplore.ieee.org/stamp/stamp.jsp?tp=&arnumber=4526021

[19] R. Love, K. Stewart, R. Bachu, and A. Ghosh, "MMSE equalization for UMTS–HSDPA," in *Proc. IEEE 58th VTC–Fall*, Oct. 2003, vol. 4, pp. 2416–2420. [Online]. Available: http://ieeexplore.ieee.org/stamp/stamp.jsp?tp=&arnumber=1285963

[20] M. Heikkila and K. Majonen, "Increasing HSDPA throughput by employing space–time equalization," in *Proc. 15th IEEE Int. Symp. PIMRC*, Sep. 2004, vol. 4, pp. 2328–2332. [Online]. Available: http://ieeexplore.ieee.org/stamp/stamp.jsp?tp=&arnumber=1368735

[21] R. Stuhlberger, L. Maurer, G. Hueber, and A. Springer, "The impact of RF impairments and automatic gain control on UMTS–HSDPA throughput performance," in *Proc. IEEE 64th VTC–Fall*, Sep. 2006, pp. 1–5. [Online]. Available: http://ieeexplore.ieee.org/stamp/stamp.jsp?tp=&arnumber=4109654

[22] M. Malkowski, "Link-level comparison of IP–OFDMA (mobile WiMAX) and UMTS–HSDPA," in *Proc. IEEE 18th Int. Symp. PIMRC*, Sep. 2007, pp. 1–5. [Online]. Available: http://ieeexplore.ieee.org/stamp/stamp.jsp?tp=&arnumber=4394134

[23] J.-B. Landre and A. Saadani, "HSDP 14,4 Mbps mobiles—Realistic throughputs evaluation," in *Proc. 67th IEEE VTC–Spring*, May 2008, pp. 2086–2090. [Online]. Available: http://ieeexplore.ieee.org/stamp/stamp.jsp?arnumber=4526024

[24] D. Samardzija, A. Lozano, and C. Papadias, "Experimental validation of MIMO multiuser detection for UMTS high-speed downlink packet access," in *Proc. 47th IEEE GLOBECOM*, Nov. 2004, vol. 6, pp. 3840–3844. [Online]. Available: http://ieeexplore.ieee.org/stamp/stamp.jsp?arnumber=1379087

[25] T. Isotalo and J. Lempiäinen, "HSDPA measurements for indoor DAS," in *Proc. 65th IEEE VTC–Spring*, Apr. 2007, pp. 1127–1130. [Online]. Available: http://ieeexplore.ieee.org/stamp/stamp.jsp?arnumber=4212667

[26] T. Isotalo, P. Lähdekorpi, and J. Lempiäinen (2008). Improving HSDPA indoor coverage and throughput by repeater and dedicated indoor system. *EURASIP J. Wireless Commun. Netw.* [Online]. *2008*, pp. 1–11. Available: http://downloads.hindawi.com/journals/wcn/2008/951481.pdf

[27] M. Jurvansuu, J. Prokkola, M. Hanski, and P. Perala, "HSDPA performance in live networks," in *Proc. IEEE ICC*, Jun. 2007, pp. 467–471. [Online]. Available: http://ieeexplore.ieee.org/stamp/stamp.jsp?arnumber=4288754

[28] H. Holma and J. Reunanen, "3GPP release 5 HSDPA measurements," in *Proc. 17th IEEE Int. Symp. PIMRC*, Sep. 2006, pp. 1–5. [Online]. Available: http://ieeexplore.ieee.org/stamp/stamp.jsp?arnumber=4022310

[29] M. Riback, S. Grant, G. Jongren, T. Tynderfeldt, D. Cairns, and T. Fulghum, "MIMO–HSPA testbed performance measurements," in *Proc. 18th IEEE Int. Symp. PIMRC*, Sep. 2007, pp. 1–5. [Online]. Available: http://ieeexplore.ieee.org/stamp/stamp.jsp?tp=&arnumber=4394434

[30] L. Hentilä, P. Kyösti, M. Käske, M. Narandzic, and M. Alatossava, MATLAB Implementation of the WINNER Phase II Channel Model ver1.1, Dec. 2007, [Online]. Available: http://www.ist-winner.org/phase_2_model.html

[31] H. Chao, Z. Liang, Y. Wang, and L. Gui, "A dynamic resource allocation method for HSDPA in WCDMA system," in *Proc. 5th IEE Int. Conf. 3G Mobile Commun. Technol. (3G)*, 2004, pp. 569–573. [Online]. Available: http://ieeexplore.ieee.org/stamp/stamp.jsp?tp=&arnumber=1434541

[32] R. Naja, J.-P. Claude, and S. Tohme, "Adaptive multiuser fair packet scheduling in HSDPA network," in *Proc. Int. Conf. IIT*, Dec. 2008, pp. 406–410. [Online]. Available: http://ieeexplore.ieee.org/stamp/stamp.jsp?tp=&arnumber=4781652

[33] R. Kwan, M. Aydin, C. Leung, and J. Zhang, "Multiuser scheduling in HSDPA using simulated annealing," in *Proc. IWCMC*, Aug. 2008, pp. 236–241. [Online]. Available: http://ieeexplore.ieee.org/stamp/stamp.jsp?tp=&arnumber=4599941

[34] C. Mehlführer and M. Rupp, "Novel tapwise LMMSE channel estimation for MIMO WCDMA," in *Proc. 51st IEEE GLOBECOM*, New Orleans, LA, Nov. 2008, pp. 1–5. [Online]. Available: http://publik.tuwien.ac.at/files/PubDat_169129.pdf

[35] C. Mehlführer, S. Caban, M. Wrulich, and M. Rupp, "Joint throughput optimized CQI and precoding weight calculation for MIMO HSDPA," in *Conf. Rec. 42nd Asilomar Conf. Signals, Syst., Comput.*, Pacific Grove, CA, Oct. 2008, pp. 1320–1325. [Online]. Available: http://publik.tuwien.ac.at/files/PubDat_167015.pdf

[36] M. Harteneck, M. Boloorian, S. Georgoulis, and R. Tanner, "Practical aspects of an HSDPA 14-Mbps terminal," in *Conf. Rec. 38th Asilomar Conf. Signals, Syst., Comput.*, Pacific Grove, CA, Nov. 2004, vol. 1, pp. 799–803. [Online]. Available: http://ieeexplore.ieee.org/stamp/stamp.jsp?arnumber=1399246

[37] M. Harteneck, M. Boloorian, S. Georgoulis, and R. Tanner (2005, Mar.). Throughput measurements of HSDPA 14-Mbit/s terminal. *Electron. Lett.* [Online]. *41(7)*, pp. 425–427. Available: http://ieeexplore.ieee.org/stamp/stamp.jsp?arnumber=1421242

[38] C. Mehlführer, S. Caban, and M. Rupp, "Measurement-based evaluation of low-complexity receivers for D-TxAA HSDPA," in *Proc. 16th EUSIPCO*, Lausanne, Switzerland, Aug. 2008. [Online]. Available: http://publik.tuwien.ac.at/files/PubDat_166132.pdf

[39] M. Wrulich, C. Mehlführer, and M. Rupp, "Interference-aware MMSE equalization for MIMO TxAA," in *Proc. 3rd ISCCSP*, St. Julians, Malta, Mar. 2008, pp. 1585–1589. [Online]. Available: http://publik.tuwien.ac.at/files/pub-et_13657.pdf

[40] C. Mehlführer, M. Wrulich, and M. Rupp, "Intracell interference-aware equalization for TxAA HSDPA," in *Proc. 3rd IEEE ISWPC*, Santorini, Greece, May 2008, pp. 406–409. [Online]. Available: http://publik.tuwien.ac.at/files/pub-et_13749.pdf

[41] M. Wrulich, C. Mehlführer, and M. Rupp (2010, Apr.). Managing the interference structure of MIMO HSDPA: A multiuser interference-aware MMSE receiver with moderate complexity. *IEEE Trans. Wireless Commun.* [Online]. *9(4)*, pp. 1472–1482. Available: http://publik.tuwien.ac.at/files/PubDat_180743.pdf

[42] Y. Guo, J. Zhang, D. McCain, and J. Cavallaro, "Efficient MIMO equalization for downlink multicode CDMA: Complexity optimization and comparative study," in *Proc. 47th IEEE GLOBECOM*, Nov. 2004, vol. 4, pp. 2513–2519. [Online]. Available: http://ieeexplore.ieee.org/stamp/stamp.jsp?arnumber=1378459

[43] Y. Guo, J. Zhang, D. McCain, and J. R. Cavallaro, An efficient circulant MIMO equalizer for CDMA downlink: Algorithm and VLSI architecture. *EURASIP J. Appl. Signal Process*. [Online]. *2006*, p. 144, Article ID 57134. Available: http://downloads.hindawi.com/journals/asp/2006/057134.pdf
[44] G. H. Golub and C. F. van Loan, Eds., *Matrix Computations*, 3rd ed. Baltimore, MD: Johns Hopkins Univ. Press, 1996.
[45] D. Garrett, G. Woodward, L. Davis, G. Knagge, and C. Nicol, "A 28.8 Mb/s 4 × 4 MIMO 3G high-speed downlink packet access receiver with normalized least-mean-square equalization," in *IEEE ISSCC Dig. Tech. Papers*, Feb. 2004, vol. 1, pp. 420–536. [Online]. Available: http://ieeexplore.ieee.org/stamp/stamp.jsp?arnumber=1332773
[46] J. Ylioinas, K. Hooli, K. Kiiskila, and M. Juntti, "Interference suppression in MIMO HSDPA communication," in *Proc. 6th NORSIG*, 2004, pp. 228–231. [Online]. Available: http://ieeexplore.ieee.org/stamp/stamp.jsp?arnumber=1344565
[47] S. Caban, C. Mehlführer, R. Langwieser, A. L. Scholtz, and M. Rupp (2006). Vienna MIMO testbed. *EURASIP J. Appl. Signal Process.—Special Issue on Implementation Aspects and Testbeds for MIMO Systems.* [Online]. *2006*, pp. 1–13, Article ID 54868. Available: http://publik.tuwien.ac.at/files/pub-et_10929.pdf
[48] S. Caban, C. Mehlführer, G. Lechner, and M. Rupp, "Testbedding MIMO HSDPA and WiMAX," in *Proc. 70th IEEE VTC–Fall*, Anchorage, AK, Sep. 2009, pp. 1–5. [Online]. Available: http://publik.tuwien.ac.at/files/PubDat_176574.pdf
[49] Kathrein, Technical Specification Kathrein Antenna Type No. 800 10629. [Online]. Available: http://www.nt.tuwien.ac.at/fileadmin/data/testbed/kat-ant.pdf
[50] C. Kakoyiannis, S. Troubouki, and P. Constantinou, "Design and implementation of printed multielement antennas on wireless sensor nodes," in *Proc. 3rd ISWPC*, Santorini, Greece, May 2008, pp. 224–228. [Online]. Available: http://ieeexplore.ieee.org/stamp/stamp.jsp?arnumber=4556202
[51] ITU, Recommendation ITU-R M.1225: Guidelines for evaluation of radio transmission technologies for IMT-2000, Geneva, Switzerland, 1997.
[52] S. Caban, C. Mehlführer, L. W. Mayer, and M. Rupp, "2 × 2 MIMO at variable antenna distances," in *Proc. 67th IEEE VTC–Spring*, Singapore, May 2008, pp. 1311–1315. [Online]. Available: http://publik.tuwien.ac.at/files/PubDat_167444.pdf
[53] C. Mehlführer, S. Caban, J. A. García-Naya, and M. Rupp, "Throughput and capacity of MIMO WiMAX," in *Conf. Rec. 43rd Asilomar Conf. Signals, Syst., Comput.*, Pacific Grove, CA, Nov. 2009, pp. 1426–1430. [Online]. Available: http://publik.tuwien.ac.at/files/PubDat_178050.pdf
[54] J. A. García-Naya, C. Mehlführer, S. Caban, M. Rupp, and L. Castedo, "Throughput-based antenna selection measurements," in *Proc. 70th IEEE VTC–Fall*, Anchorage, AK, Sep. 2009, pp. 1–5. [Online]. Available: http://publik.tuwien.ac.at/files/PubDat_176573.pdf
[55] B. Efron and D. V. Hinkley, *An Introduction to the Bootstrap (CRC Monographs on Statistics and Applied Probability 57)*, 1st ed. London, U.K.: Chapman & Hall, 1994.
[56] C. Mehlführer, S. Caban, and M. Rupp, Experimental evaluation of adaptive modulation and coding in MIMO WiMAX with limited feedback. *EURASIP J. Adv. Signal Process.—Special Issue on MIMO Systems With Limited Feedback*. [Online]. *2008*, pp. 1-12, Article ID 837102. Available: http://publik.tuwien.ac.at/files/pub-et_13762.pdf
[57] I. E. Telatar (1999, Nov./Dec.), Capacity of multiantenna Gaussian channels. *Eur. Trans. Telecommun., Tech. Memo., Bell Labs. Lucent Technologies*. [Online]. vol. 10, no. 6, pp. 585-595. Available: http://mars.bell-labs.com/papers/proof/proof.pdf
[58] G. J. Foschini and M. J. Gans (1998, Mar.), On limits of wireless communications in a fading environment when using multiple antennas. *Wireless Pers. Commun.* [Online]. vol. 6, no. 3, pp. 311-335. Available: http://www.springerlink.com/content/h1n7866218781520/fulltext.pdf
[59] G. G. Raleigh and J. M. Cioffi (1998, Mar.), Spatiotemporal coding for wireless communication. *IEEE Trans. Commun.* [Online]. vol. 46, no. 3, pp. 357-366. Available: http://www-isl.stanford.edu/~cioffi/dsm/wlpap/mimocioffi98.pdf
[60] A. Paulraj, R. Nabar, and D. Gore, *Introduction to Space–Time Wireless Communications*, 1st ed. Cambridge, U.K.: Cambridge Univ. Press, 2003.
[61] M. Rupp, C. Mehlführer, and S. Caban, "On achieving the Shannon bound in cellular systems," in *Proc. 20th Int. Conf. Radioelektronika*, Brno, Czech Republic, Apr. 2010, pp. 1–5, invited. [Online]. Available: http://publik.tuwien.ac.at/files/PubDat_185403.pdf
[62] M. Rupp, J. A. García-Naya, C. Mehlführer, S. Caban, and L. Castedo, "On mutual information and capacity in frequency-selective wireless channels," in *Proc. IEEE ICC*, Cape Town, South Africa, May 2010, pp. 1–5. [Online]. Available: http://publik.tuwien.ac.at/files/PubDat_184660.pdf

Christian Mehlführer (M'09) was born in Vienna, Austria, in 1979. He received the Dipl.Ing. degree in electrical engineering from the Vienna University of Technology in 2004. After finishing his Diploma thesis on implementation and real-time testing of space-time block codes with the Institute of Communications and Radio-Frequency Engineering, Vienna University of Technology, for which he received the 2006 Vodafone Förderpreis, he started his Ph.D. dissertation on measurement-based performance evaluation of WiMAX and High-Speed Downlink Packet Access (HSDPA). He received the Ph.D. degree from the Vienna University of Technology in 2009.

During his Diploma studies, he worked part time with Siemens AG, where he performed integration tests of Global System for Mobile Communications carrier units. He is currently with the Institute of Communications and Radio-Frequency Engineering, Vienna University of Technology. His research interests include experimental investigation of multiple-input–multiple-output systems, Universal Mobile Telecommunications System HSDPA, WLAN (802.11), WiMAX (802.16), and the upcoming Third-Generation Partnership Program Long-Term Evaluation LTE system.

Sebastian Caban (M'09) was born in Vienna, Austria, on March 13, 1980. He went to a technical high school and received the Bachelor's degree in electrical and communication engineering from the Vienna University of Technology. He received the Master's degree in 2005 and the Ph.D. degree in 2009. In between, he spent a year with the University of Illinois at Urbana-Champaign. He received the B.B.A. and M.B.A. degrees, with a major in economics, from the University of Vienna in 2010.

He is currently with the Institute of Communications and Radio-Frequency Engineering, Vienna University of Technology. His research interests include developing measurement methodologies and building testbeds to quantify the actual performance of wireless cellular communication systems (e.g., Universal Mobile Telecommunications System and Long-Term Evaluation) in realistic scenarios.

Dr. Caban received 12 national scholarships and prizes and the Förderpreis 2006 from the German Vodafone Stiftung für Forschung for his research.

Markus Rupp (SM'06) received the Dipl.Ing. degree from the University of Saarbrücken, Saarbrücken, Germany, in 1988 and the Dr.Ing. degree from Technische Universität Darmstadt, Darmstadt, Germany, in 1993, where he worked with E. Hänsler on designing new algorithms for acoustical and electrical echo compensation.

From November 1993 to July 1995, he held, with S. Mitra, a postdoctoral position with the University of California, Santa Barbara, where he worked with A. H. Sayed on a robustness description of adaptive filters with impact on neural networks and active noise control. From October 1995 to August 2001, he was a Member of Technical Staff with the Wireless Technology Research Department, Bell Laboratories, Crawford Hill, NJ, where he worked on various topics related to adaptive equalization and rapid implementation for IS-136, 802.11, and the Universal Mobile Telecommunications System. Since October 2001, he has been a Full Professor of digital signal processing in mobile communications with the Vienna University of Technology, where he founded the Christian Doppler Laboratory for Design Methodology of Signal Processing Algorithms, at the Institute of Communications and Radio-Frequency Engineering, in 2002. He served as Dean from 2005 to 2007. He is currently an Associate Editor for the *JASP EURASIP Journal of Advances in Signal Processing* and the *JES EURASIP Journal on Embedded Systems*. He is the author or a coauthor of more than 300 papers and is the holder of 15 patents on adaptive filtering, wireless communications, and rapid prototyping, as well as automatic design methods.

Dr. Rupp was an Associate Editor for the IEEE TRANSACTIONS ON SIGNAL PROCESSING from 2002 to 2005. He has been an Administrative Committee Member of EURASIP since 2004 and served as the President of EURASIP from 2009 to 2010.